ELSEVIER

Contents lists available at ScienceDirect

# Electrochimica Acta

journal homepage: www.elsevier.com/locate/electacta



# Electrochemical behavior of praseodymium on the W and Al–Zn electrodes in LiCl–KCl eutectic: A comparison study



Ya-lan Liu <sup>a, 1</sup>, Hao Ren <sup>a, 1</sup>, Tai-qi Yin <sup>a</sup>, Da-wei Yang <sup>a</sup>, Zhi-fang Chai <sup>a, b</sup>, Wei-qun Shi <sup>a, \*</sup>

- <sup>a</sup> Laboratory of Nuclear Energy Chemistry, Institute of High Energy Physics, Chinese Academy of Sciences, Beijing, 100049, China
- <sup>b</sup> Engineering Laboratory of Advanced Energy Materials, Ningbo Institute of Industrial Technology, Chinese Academy of Sciences, Ningbo, Zhejiang, 315201, China

#### ARTICLE INFO

Article history:
Received 19 July 2019
Received in revised form
25 September 2019
Accepted 27 September 2019
Available online 30 September 2019

Keywords: Electrodeposition Praseodymium Al–Zn binary cathode Molten salt

#### ABSTRACT

A new active Al–Zn electrode for recovering praseodymium (Pr) from spent nuclear fuel in chloride molten salts was proposed in this work. The electrochemical behavior of Pr(III) ions dissolved in LiCl–KCl eutectic and its co-reduction with Al(III) and Zn(II) ions on the W electrode as well as its reduction at the liquid Al–Zn electrode were studied and compared. In addition, the diffusion coefficient of Pr(III) ions in melt was evaluated using semi-integral and semi-differential techniques, respectively. The results showed that the number of redox signals corresponding to Pr–Zn intermetallic compounds are more than that for Pr–Al intermetallics. Potentiostatic and galvanostatic electrolysis were both carried out on various electrodes to identify the formation of different Pr-containing alloys. The characterizations for cathodic deposits obtained were accomplished by using X-ray diffraction (XRD) and scanning electron microscopy with energy dispersive spectroscopy (SEM-EDS). The work described here can broaden the applications of Al–Zn alloys and highlight its potentials in future molten salt electrolysis based spent fuel pyroprocessing.

© 2019 Elsevier Ltd. All rights reserved.

### 1. Introduction

Pyrochemical reprocessing of spent nuclear fuel (SNF) primarily intends to reprocess the advanced fuels and transmutation blankets which reach very high burn-ups and are expected to contain high level of Pu and minor actinides (MAs) [1–5]. Typically, the key step in the pyrochemical reprocessing is the molten salt electrorefining, in which most actinides (Ans) are recovered and decontaminated from the fission products (FPs) [2,6]. During the electrorefining process, the chemically active FPs exchange with the actinide chlorides in melt and afterwards the concentration for FPCl<sub>x</sub> gradually increases [7]. Consequently, to avoid lowering the actinide/FPs separation efficiency and be conducive for cyclic utilization of the electrolyte, the molten chlorides media must be regularly purified or regenerated when the FPCl<sub>x</sub> concentration exceeds roughly 10 wt% in LiCl–KCl eutectic salt [8].

Praseodymium, which exists in molten salt in the form of trivalent ion Pr(III), is a typical fission element and difficult to be

removed from actinides. To recover and separate praseodymium from actinides, it is of much significance to investigate the electrochemistry of Pr(III) for in-depth understanding the separation process of lanthanides (Lns) and Ans. Up to now, several groups explored the electrochemical properties of Pr(III) in molten chlorides [9–12]. Particularly, various kinds of active cathode materials have been carried out to extract praseodymium, such as Al [9,12–14], Zn [15,16], Bi [17–19], Cd [17,20], Mg [21] and Ni [10,22,23], allowing Pr(III) ions to be reduced at more anodic potentials via forming Pr alloys, which affords a mild and convenient approach for the electrolysis.

Investigations on the distribution of Ans and Lns between liquid Al metal/Al—Cu alloy and molten fluoride melts has demonstrated that the strong interaction between Ans and the liquid Al alloys might lead to the excellent recovery efficiency of Ans over Lns [24—26]. In recent years, our group has also employed an Al electrode to achieve the separation of Ans from Lns, and effective recovery of Ans has been attained with a high An/Ln separation factor [27—33]. However, at the temperature of the normal electrorefining process, the Al electrode is in solid form, and An or Ln elements will form an alloy on the cathode surface and continuously diffuse into the interior Al bulk. As such, the entire process is largely controlled

<sup>\*</sup> Corresponding author.

E-mail address: shiwq@ihep.ac.cn (W.-q. Shi).

<sup>&</sup>lt;sup>1</sup> These authors contributed equally to this work.

by the diffusion of metal into the interior of the electrode. On the other hand, zinc, as one of the active cathode materials, has attracted considerable attention towards the recovery of Lns from molten salt [15,16,34–37], since the lower melting point (692.65 K) and boiling point (1180.15 K) for zinc enable the recovery process to be conducted at relatively lower temperatures, to some extent, which can lower the melting point of Al based on the Al–Zn binary phase diagram and compensate for the disadvantage of using Al as a cathode.

Hence, in this work, to recover praseodymium from molten LiCl—KCl salt more efficiently, we propose an electrochemical extraction method for Pr assisted with Al and Zn together, and the present work focuses on the Pr electrochemistry at both the solid W and liquid Al—Zn electrodes as well as on making clear the formation process and related mechanisms regarding Pr-Al–Zn intermetallic compounds.

# 2. Experimental

### 2.1. General features

Anhydrous LiCl, KCl, BiCl<sub>3</sub>, AlCl<sub>3</sub> and ZnCl<sub>2</sub> (A.R. grade) were purchased from Sinopharm Chemical Reagent Co., Ltd, while praseodymium metal (>99.9%) came from Alfa Aesar. The experimental cell consists of a straight wall alumina crucible placed in a cylindrical quartz cell inside an electric furnace, and during the experiment the salt temperature was monitored with a nickel-chromium thermocouple and kept to  $\pm 1$  K. Moreover, storage and operations for all reagents were treated under inert argon atmosphere to avert exposure of oxygen and moisture. The concentrations of oxygen content and moisture levels were controlled to be less than 1 ppm.

## 2.2. Electrochemical electrodes

All of the electrodes and thermocouple were positioned in molten salt using a custom-built quartz structure. Unless otherwise stated, the potentials were referred to this Ag/Ag<sup>+</sup> couple, which was fabricated from a silver wire (Alfa Aesar, 99.99% purity,  $\phi = 1 \text{ mm}$ ) dipped into the solution of AgCl (1 wt%) in LiCl-KCl melts contained in an closed-end alumina tube, playing a role of a reference electrode (RE). As for the counter electrode (CE), a 6 mm diameter graphite rod was used. AW wire (Alfa Aesar, 99.9% purity) sheathed with an alumina tube of 1 mm in diameter served as the working electrode (WE). Prior to run, the working electrode was cleaned by galvanostatic anodic polarization and polished by fine sand paper in case of necessity. The active W electrode surface area  $(S = 0.56 \text{ cm}^2)$  was calculated after each experiment via measuring the length of the working electrode submerged into the melts. Moreover, the liquid Al–Zn electrode ( $S \approx 0.97 \text{ cm}^2$ ) with the eutectic composition (15 wt.% Al) was prepared by fusing pure individual metals (Al > 99.99% and Zn > 99.99%) in the glove box. To make the alloy more uniform, we stirred the liquid Al-Zn alloy during the fusing process.

#### 2.3. Melt preparation and electrochemical measurements

The eutectic LiCl–KCl (45:55 wt%) was dried under vacuum for more than 48 h at 473 K to get rid of residual water. Praseodymium metal block was used as the raw material of Pr(III) ions following the reaction according to Ref. [19], which elaborates praseodymium metal could be chlorided by BiCl<sub>3</sub> oxidant with praseodymium chloride yielded. This reaction could be expressed as:

$$BiCl_3 + Pr = Bi + PrCl_3 \tag{1}$$

BiCl<sub>3</sub> is a volatile salt that will rapidly volatilize at about 500 °C and would be thus introduced into LiCl-KCl eutectic directly. At the same time, Pr metal block connected with a molybdenum wire was also directly put into molten salt. In order to increase the contact area between the BiCl<sub>3</sub> and Pr metal block, we continuously shook the molybdenum wire connected with Pr metal. As for the amount of BiCl<sub>3</sub> added into the system, there was absolutely excess of Pr metal in the cell, so there will be no Bi(III) ions impurities in molten salt system, and the green color of the melt proved the generation of Pr(III) ions. The reaction was ended until the Bi element was not detected in molten LiCl-KCl eutectic by inductively coupled plasma atomic emission spectrometer (ICP-AES Perkin Elemer NEXION 300D) and the Pr metal block should be lifted up from molten salt by a molybdenum wire. Actually, for convenience, higher concentration of PrCl<sub>3</sub> in LiCl–KCl molten salt was prepared. In the light of different studied objects and purposes, the yielded LiCl-KCl-PrCl<sub>3</sub> salts with higher concentration was added to the LiCl-KCl eutectic and diluted to the desired concentration for experimental investigation.

All electrochemical measurements were executed with an Autolab PGSTAT 302 N electrochemical workstation controlled with the Nova 1.11 software package.

### 2.4. Preparation and characterization of cathodic deposits

Specimens of Pr-Al-Zn alloys were prepared by electrolysis using molybdenum net  $(10 \times 15 \times 0.1 \text{ mm}, 200 \text{ mesh})$  and/or liquid Al–Zn alloy as cathode, the graphite rod of 6 mm diameter as anode. The cathodic deposits were drawn out from the bath and washed ultrasonically with ethanol, which scarcely reacts with Pr-Al-Zn alloys, to remove solidified salt attached to their surfaces and afterwards stored in the glove box before subjected to further analyses. The cathodic deposits were characterized by X-ray diffraction (XRD, Bruker, D8 Advance). The composition and structure of Pr-Al-Zn samples were examined by utilizing scanning electron microscopy (SEM, Hitachi S-4800) coupled with energy dispersive spectrometry (EDS, GENESIS 2000).

### 3. Results and discussion

# 3.1. Electrochemical behaviour of praseodymium on solid W electrode

Cyclic voltammogram (CV) measurements on the W electrode were carried out at 723 K. Fig. 1a elucidates a series of CV curves in LiCl–KCl eutectic before (pink curve) and after (gray curve) the PrCl $_3$  (1.1 wt%) introduction. The cathodic signal A at appropriately  $-2.55\,\mathrm{V}$  and its corresponding striping signal A', are due to the formation and depletion of lithium metal, respectively [16,35]. As can be seen, when PrCl $_3$  is present in LiCl–KCl eutectic, one couple of cathodic/anodic signals, B/B', emerge in the voltammogram. The sharp cathodic wave B shows that the cathodic deposit at close to  $-2.00\,\mathrm{V}$  is an insoluble phase with respect to the formation of Pr metal.

Moreover, the "crossover" phenomenon is observed in the cyclic voltammogram recorded at a lower scan rate of 20 mV/s (see Fig. 1a inset), manifesting that it was the result of surface area growth caused by metal dendrite formation or that nucleation was involved in the reduction process [38–40], similar phenomena have been also reported previously in the reduction process of Mg(II) [41] and U(III) [42].

On the other hand, the potential value of signal B gradually shifts towards more negative direction and that the associated peak current increases continuously along with the rise of scan rate, as depicted in Fig. 1a. The reason for this behavior may be the

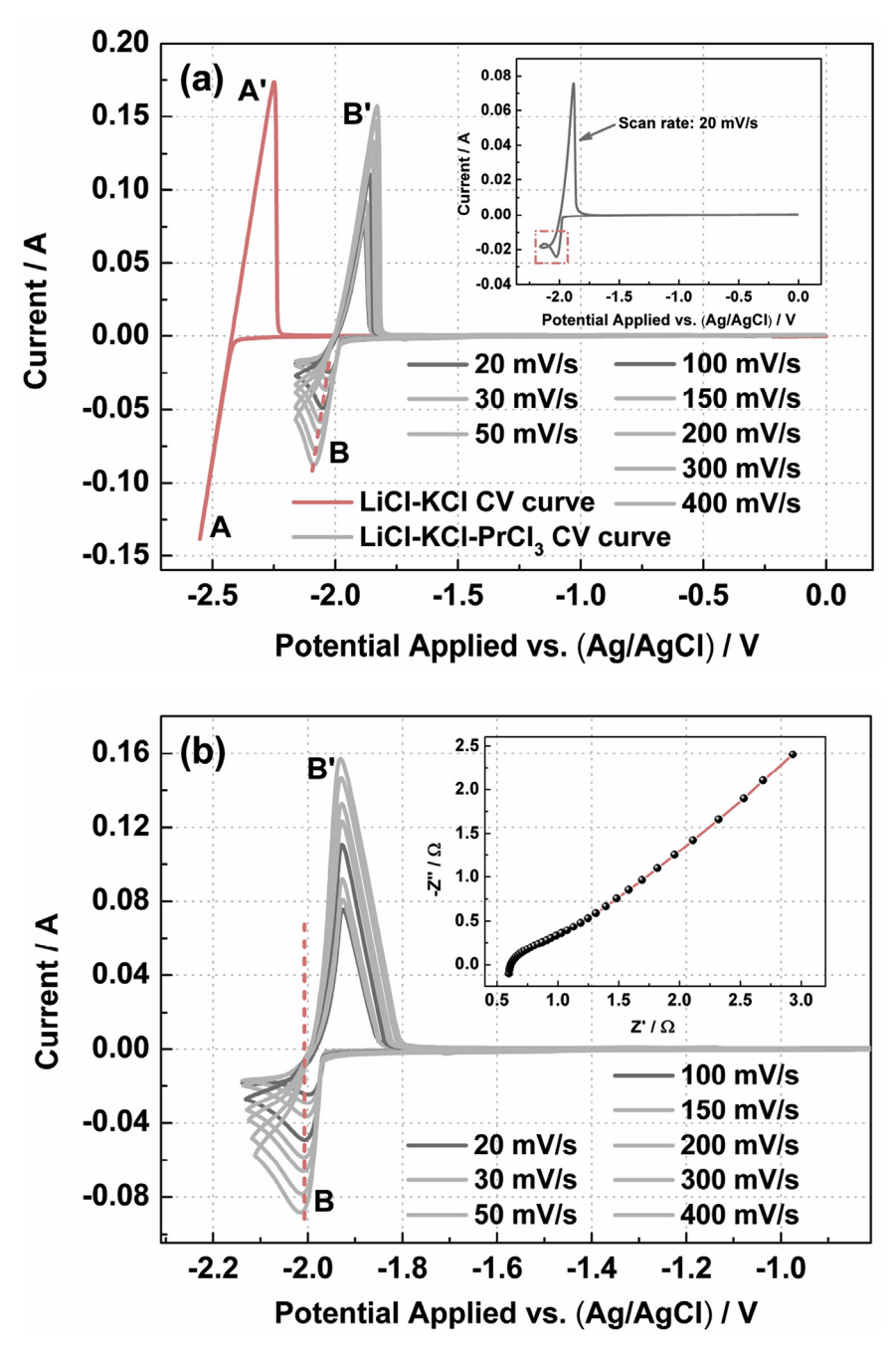


**Fig. 1.** (a) CV curves on the W electrode recorded before (pink curve) and after (gray curve) the addition of PrCl<sub>3</sub> (1.1 wt%) the LiCl–KCl eutectic. Temperature: 723 K. Inset: CV curve obtained in LiCl–KCl-PrCl<sub>3</sub> (1.1 wt%) molten salt on the W electrode with various scan rates. Temperature: 723 K. Inset: EIS obtained at open circuit potential. (For interpretation of the references to color in this figure legend, the reader is referred to the Web version of this article.)

influence of ohmic drop which varies with the scan rate and also is a function of the cathodic current because of the electrolyte resistance [28,43]. In Fig. 1b (inset), the electrolyte resistance was measured to be  $0.61\,\Omega$  via electrochemical impedance spectroscopy (EIS). Fig. 1b shows a group of CV curves obtained in the LiCl–KCl-PrCl<sub>3</sub> molten salt at various scan rates after doing ohmic compensation, at 723 K. The cathodic peak potentials are almost independent on the scan rate and locate at around  $-2.01\,\text{V}$ .

According to Ref. [44], Haarberg et al. demonstrated that the Berzin-Delahay equation would be invalid since the electrode was not covered by multiple monolayer products in the deposition process. Another alternative approach is to convolute the cyclic voltammetric data, afterwards, the semi-integral curve is very similar to the steady-state voltammetric curve, which provides convenience for further data analysis [45–48]. The semi-integral curve of the voltammetric data can be given by applying the

following expression:

$$\mathbf{m}(t) = \frac{d^{-1/2}}{dt^{-1/2}}i(t) = \frac{1}{\pi^{1/2}} \int_{0}^{t} \frac{i(\tau)}{(t-\tau)^{1/2}} dt$$
 (1)

where  $i(\tau)$  denotes the current of the CV, m(t) presents the semi-integral current.

The current of a representative semi-integral curve (Fig. 2 pink curve) obtained from the CV curve with the scan rate of 100 mV/s reaches a semi-integral limiting value, 0.0528, as shown in Fig. 2. For Pr(III)/Pr couple, this diffusion coefficient can be evaluated from  $m^*$  per Eq. (2):

$$m * = -nFSC_0D^{1/2} \tag{2}$$

where m\* represents semi-integral limiting current, n corresponds to the number of electrons, S is the electrode surface area,  $C_0$  the concentration of Pr(III), D designates the diffusion coefficient. Hence, the diffusion coefficient of Pr(III) is determined to be  $2.02\times 10^{-5}\, {\rm cm^2/s}$  by convolution voltammetry, which is higher than that published in Ref. [22], and the diffusion coefficients calculated from the convoluted curves for different scan rates are shown in Table 1. With these characteristics the forward and backward scans are not coincident and the hysteresis phenomenon takes place, the electrode reaction for Pr(III) on the W electrode might be not fully reversible [48,49].

# 3.2. Electrochemical behaviour of praseodymium at liquid Al–Zn electrode

Further, the electrochemical behaviour for praseodymium chloride in eutectic LiCl–KCl molten salts at liquid Al–Zn electrode was studied. In Fig. 3, the blue curve (1) shows the results collected at the liquid Al–Zn electrode in the blank LiCl–KCl melt, with a scan rate of 50 mV/s. The electrochemical window at liquid Al–Zn electrode (blue curve 1) is much narrower than that on inert W electrode (about 1.0 V). The cathodic limit for CV curve derives from the lithium reduction at liquid Al–Zn electrode (signal B, Li–Al alloy or Li–Zn alloy), whereas the anodic one is associated with the anodic dissolution process of the liquid Al–Zn electrode (signal A'). As for the pink curve (2), one new cathodic wave C and its corresponding striping wave C' were detected at around –1.29/-0.82 V after PrCl<sub>3</sub> was added into the LiCl–KCl system, owing to the deposition and depletion of praseodymium metal at the liquid Al–Zn electrode, respectively. In addition, we can find that there is

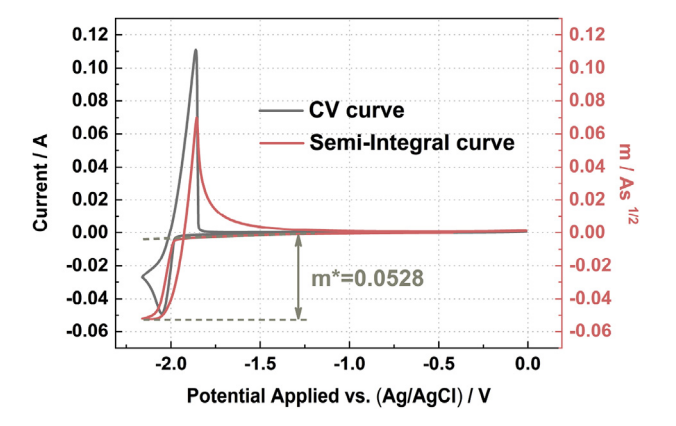
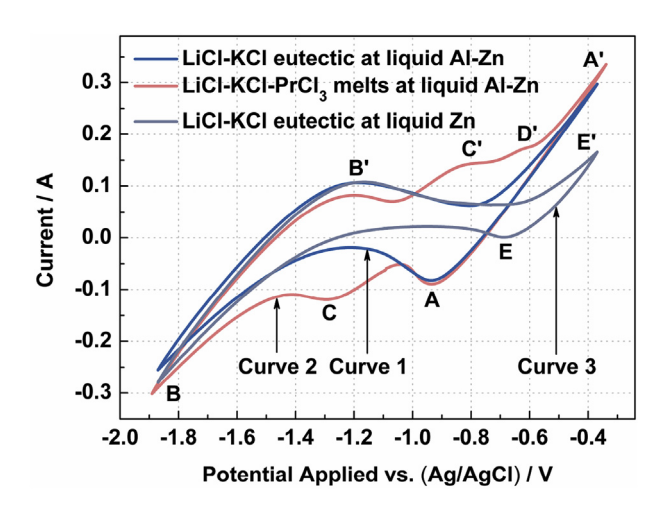


Fig. 2. Convoluted voltammogram gained in the LiCl-KCl-PrCl $_3$  (1.1 wt%) melts on the W electrode at 723 K, Scan rate:  $100\,\text{mV/s}$ .

Table 1 Diffusion coefficient of Pr(III) ions in LiCl–KCl eutectic at different scan rates. (D  $\times\,10^5$  cm²/s).

Scan rate/mV/s	50	100	150	200	250	300	400
Cyclic voltammetry Convolution	2.21 3.84	2.02 4.53	1.92 5.04	1.89 6.61	6.9	1.83	1.79



**Fig. 3.** CVs obtained at liquid Al–Zn electrode in LiCl–KCl eutectic without/with PrCl<sub>3</sub> (2.02 wt%) (curve 1, 2) and collected at a liquid Zn electrode (curve 3) in LiCl–KCl eutectic. Temperature: 783 K; Surface area: 0.97 cm²; Scan rate: 50 mV/s.

one more anodic signal (D') during the backward scan, and the similar phenomenon was detected during the Ln reduction process [50].

In surprise, within the electrochemical window range, only the reduction signal arising from Al(III) ions is detected, and the reduction signal of Zn(II) ions at the liquid Al–Zn electrode vanishes. The CV measurement was thus carried out in molten LiCl–KCl eutectic at the liquid Zn electrode, and the results were displayed in Fig. 3 (curve 3). Comparing curve 3 with curve 1, an anodic peak E' at  $-0.37\,\mathrm{V}$  corresponding to the anodic oxidation of liquid zinc electrode, related to a well-defined cathodic one E is observed. The reason why the reduction peak for Zn vanished at the liquid Al–Zn electrode may be that the reduction peak of Al(III) is too large, and thus the reduction signal B is caused by the Li–Zn alloy [51].

One of the most sensible answers with respect to the reversibility for a redox reaction, will be generally found via the application of peak-voltammetry theories [52]. As shown in Fig. 4a, with scan rate increasing, the cathodic and anodic signals shift slightly to more cathodic and anodic values, respectively. Fig. 4a inset presents the variation of the peak potentials for C/C' couple versus logarithm of the scan rate. The peak potential alterations with regard to signals C/C' are insignificant at scan rates below 50 mV/s, manifesting the redox reaction of Pr(III) at the liquid Al-Zn electrode may incline towards being reversible; whereas for the scan rate up to 250 mV/s,  $\Delta E_c$  and  $\Delta E_a$  will be significantly increased and two linear relationships of the redox peak potentials as a function of the logarithm of the scan rate illustrate, which suggests that the overall electrode reaction of Pr(III) ions to metal Pr should be considered to be a quasi-reversible process. Fig. 4b shows a group of CV curves obtained in the LiCl-KCl-PrCl<sub>3</sub> molten salt at various scan rates after doing ohmic compensation, at 723 K. It can be observed that the cathodic peak B potentials of the CV curves consistently shift to slightly more negative values, manifesting the possible presence of electron transfer rate control component during the overall redox

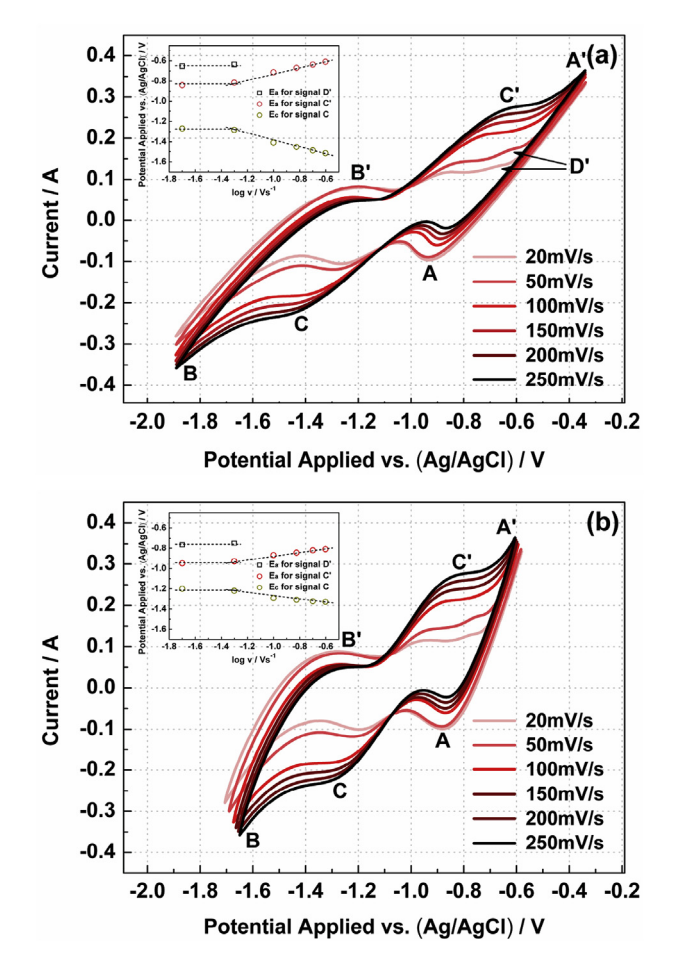


**Fig. 4.** (a) CV curves for  $2.02 \text{ wt}\% \text{ PrCl}_3$  in LiCl–KCl eutectic salts at the liquid Al–Zn electrode with various scan rates (20-250 mV/s). Inset: Variation of the cathodic and anodic peak potential with the logarithm of the scan rate; (b) CV curves after correction for ohmic drop in terms of LiCl–KCl-PrCl $_3$  (2.02 wt%) molten salt at the liquid Al–Zn electrode with various scan rates. Temperature: 723 K.

### reaction [40,53].

Because of the large background current at the liquid Al–Zn electrode, the reduction peak current of signal C in Fig. 4 actually is not distinguishable, from which it is of considerable difficulty to obtain the diffusion coefficient of Pr(III) directly due to the possible errors about peak current determination. In consequence, the CV curve is further processed by semi-differential technique, and related equation is described as follows:

$$e(t) = \frac{d^{1/2}}{dt^{1/2}}i(t) = \frac{d}{dt}(\frac{1}{\sqrt{\pi}}\int_{0}^{t} \frac{i(u)}{\sqrt{t-u}}du)$$
 (3)

where i(t) donates the current of the CV, e(t) designates the semi-differential current.

Fig. 5a shows a representative semi-differential curve derived from CV curve recorded in LiCl–KCl-PrCl<sub>3</sub> melt at the liquid Al–Zn pool electrode. It is observed that the reduction peak of the semi-differential curve is more clear and obvious, and has higher accuracy on confirming its peak current as well. Therefore, according to the semi-differential theories, the diffusion coefficient can be

estimated using Eqs. (4) and (5):

$$W_{\rm p} = \frac{2.94RT}{\alpha {\rm nF}} \tag{4}$$

$$e_{p} = \frac{\alpha n^{2} F^{2} Sv C_{0} D^{1/2}}{3.367 RT}$$
 (5)

where F, R and T have the usual meanings, Wp and ep represent peak width and peak height, respectively. The peak width (W<sub>n</sub>) concerning cathodic signal C is measured to be 0.343. With subsequent the conversion calculation, it is also discovered that the kinetic parameter ' $\alpha$ n' value is equal to 0.58 for reduction of Pr(III). The peak height, ep decreases in proportion to the scan rate which is shown in Fig. 5b. Based on the slope of the fitted curve, the calculated value of diffusion coefficient here is determined to be  $4.53 \times 10^{-5} \, \text{cm}^2/\text{s}$ , and for the scan rates of 50, 150, 200 and 250 mV/s, the diffusion coefficients for Pr(III) ions are given in Table 1, which are generally higher than these obtained on the W electrode, indicating that the electrode material has a some influence on the diffusion coefficient of Pr(III) ions. Furthermore, this slight discrepancy with respect to the diffusion coefficients between the W and liquid Al-Zn electrodes might be due to the systematic error in the surface area determination of the liquid Al-Zn electrode as well.

# 3.3. Electrochemical behaviour of Pr(III), Al(III) and Zn(II) in LiCl–KCl eutectic on the W electrode

For the purpose of getting more details in terms of the intermetallic compound formation, the co-reduction process for Pr(III), Al(III) and Zn(II) ions on the W electrode were investigated as well. Fig. 6a exhibits the comparison of typical CV curves recorded in the LiCl-KCl eutectic containing ZnCl<sub>2</sub> (0.2 wt%), PrCl<sub>3</sub> (1.1 wt%) and ZnCl<sub>2</sub> (0.2 wt%)-PrCl<sub>3</sub> (1.1 wt%), respectively. Two redox couples A/ A' and C/C' (see Fig. 6a), associated with the deposition and its subsequent dissolution reaction of lithium and zinc metals, respectively, can be detected in LiCl-KCl-ZnCl2 system. When PrCl<sub>3</sub> is present in molten LiCl-KCl-ZnCl<sub>2</sub> melts, except for the A/A' and C/C' redox systems described previously, five various waves labeled with D/D', E/E', F/F', G/G' and H/H', are discovered at -1.33/-1.21 V, -1.76/-1.55 V, -1.85/-1.70 V, -1.88/-1.74 V and -1.97/-1.82 V, respectively. Here, the five different kinds of redox signals are located within the electrochemical window limited by the reduction of Pr(III) (signal B) and the reoxidation of metallic Zn to Zn(II) ions (signal C'), and should be ascribed to the deposition/ dissolution of Pr–Zn intermetallic compounds.

In the case of the gray curve in Fig. 6b, the CV test was performed in LiCl—KCl eutectic with a solution of both of ZnCl<sub>2</sub> and AlCl<sub>3</sub> on the W electrode at 723 K. Three redox peaks A/A', C/C' and I/I' are correlated to the formation and dissolution of metallic lithium, zinc and aluminum, respectively. Unexpectedly, between peaks C/C' and I/I', one sharp anodic peak X' appears, probably due to depletion of the unstable Al—Zn alloy. The cyclic voltammogram consists of five new redox couples after PrCl<sub>3</sub> addition into the molten LiCl—KCl—AlCl<sub>3</sub>—ZnCl<sub>2</sub> melts, as shown in Fig. 6b red curve, arising from the Pr-Al-Zn alloys. Compared with LiCl—KCl-PrCl<sub>3</sub>-ZnCl<sub>2</sub> system (i.e. the comparison of the blue curve in Fig. 6a with Fig. 6b red curve), it is reasonable to suggest that the redox couples D/D', F/F' and H/H' in Fig. 6b are interpreted as the formation and dissolution for three kinds of Pr—Zn intermetallic compounds, however,

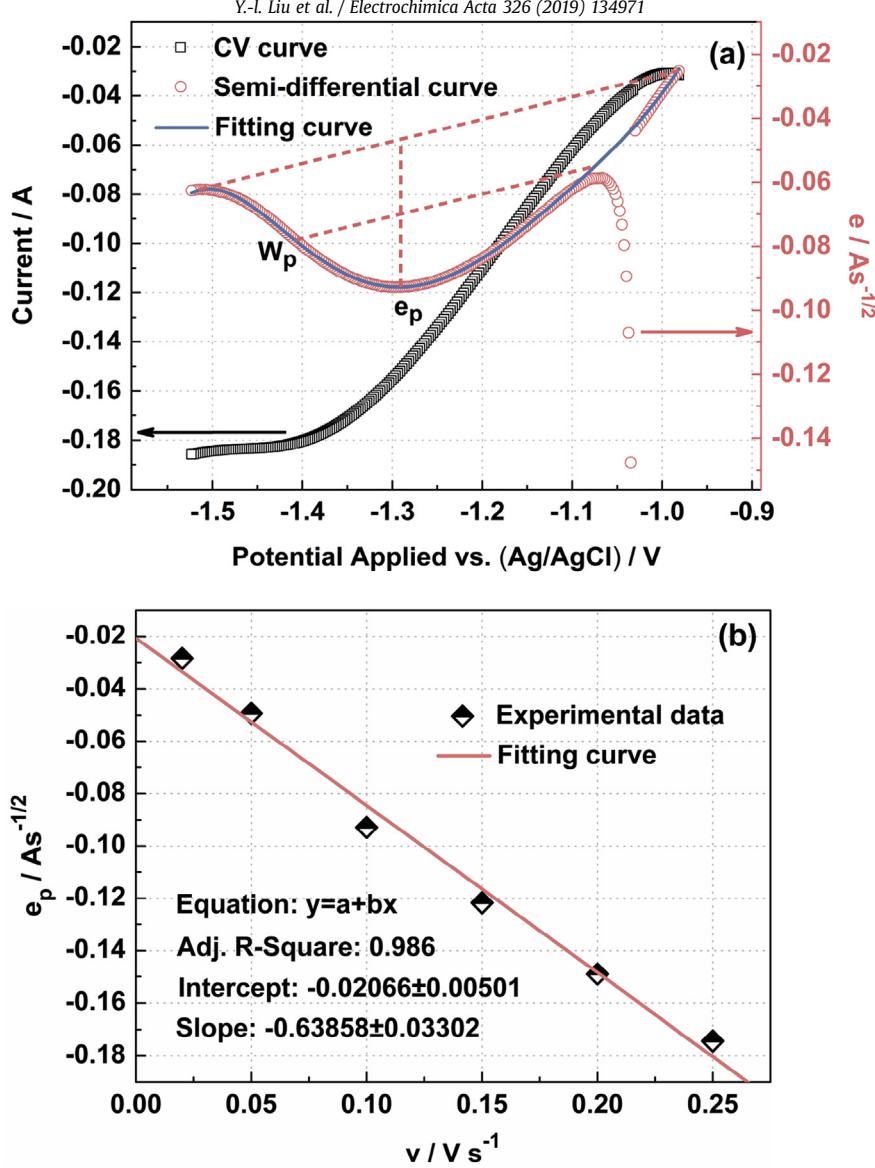


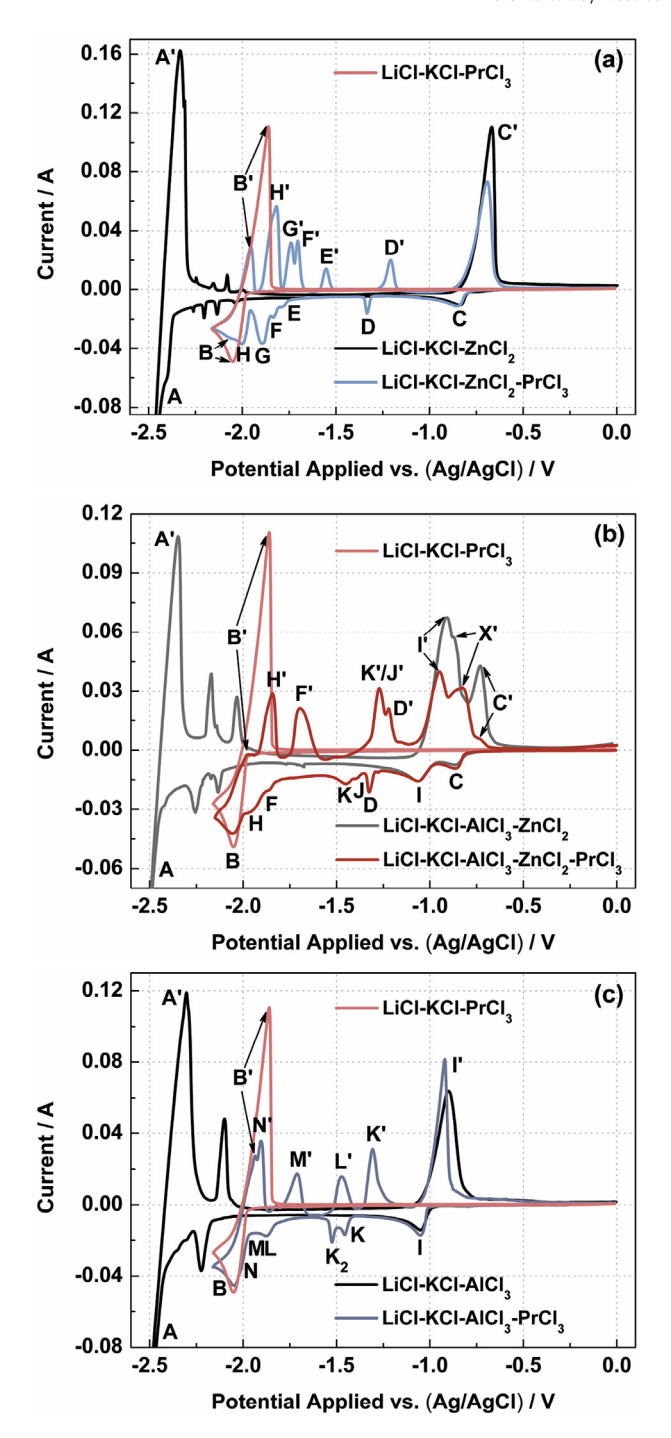
Fig. 5. (a) Convoluted voltammogram obtained in the LiCl-KCl-PrCl<sub>3</sub> (2.02 wt%) melt at the liquid Al-Zn electrode. Scan rate: 100 mV/s. (b) The relationship of ep with the scan rate. Temperature: 783 K.

Table 2 Summary of the results collected by CV and OCP techniques on the W electrode in LiCl-KCl-PrCl<sub>3</sub>-ZnCl<sub>2</sub>-AlCl<sub>3</sub> system at 723 K.

CV		OCP		
Signal	Potential/V	Plateau	Potential/V	
В	-2.04	В	-1.98	
C	-0.86	С	-0.81	
D	-1.33	D	-1.25	
E	-1.76	E	-1.60	
F	-1.85	F	-1.75	
G	-1.88	G	-1.79	
Н	-1.97	Н	-1.87	
I	-1.05	I	-1.02	
J	-1.38	J	-1.32	
K	-1.45	$K_2/K_4$	-1.34	
$K_2$	-1.53	K <sub>2</sub> '	-1.54	
L	-1.87	L	-1.79	

what substances peaks J/J' and K/K' belong to is still a question. Keeping this in mind, some voltammetric data were also employed to summary the redox couple potentials of Pr-Al intermetallic compounds.

The black curve of Fig. 6c illustrates an example of the cyclic voltammogram recorded on the W electrode in the LiCl-KCl-AlCl<sub>3</sub> molten salt. In consequence, a cathodic wave I is observed at  $-1.05\,V$  and its corresponding sharp anodic wave I' at  $-0.90\,V$ 



**Fig. 6.** The CV curves obtained on the W electrode at 723 K in different molten salt systems: (a) black curve: LiCl–KCl–ZnCl<sub>2</sub> (0.2 wt%) melts, pink curve: LiCl–KCl-PrCl<sub>3</sub> (1.1 wt%) melts, blue curve: LiCl–KCl-PrCl<sub>3</sub> (1.1 wt%)-ZnCl<sub>2</sub> (0.2 wt%) melts; (b) gray curve: LiCl–KCl–ZnCl<sub>2</sub> (0.2 wt%)-AlCl<sub>3</sub> (0.2 wt%)-AlCl<sub>3</sub> (0.2 wt%)-AlCl<sub>3</sub> (0.2 wt%)-AlCl<sub>3</sub> (0.2 wt%)-ZnCl<sub>2</sub> (0.2 wt%) melts, cc) black curve: LiCl–KCl–AlCl<sub>3</sub> (0.2 wt%) melts, purple curve: LiCl–KCl–PrCl<sub>3</sub> (1.1 wt%)-AlCl<sub>3</sub> (0.2 wt%) melts. Temperature: 723 K; Scan rate: 100 mV/s. (For interpretation of the references to color in this figure legend, the reader is referred to the Web version of this article.)

are attributed to the formation of aluminum metal and dissolution reaction. When PrCl<sub>3</sub> was introduced into the LiCl–KCl–AlCl<sub>3</sub> melts, five pairs of new cathodic signals and their corresponding anodic signals occurred (the purple curve, Fig. 6c). On the basis of Refs. [12,14], Tang et al. concluded that the redox signals (K/K', L/L' and M/M') could be caused by the reduction and reoxidation of

Pr—Al alloys in the LiCl—KCl-PrCl<sub>3</sub>-AlCl<sub>3</sub> system. Howover, we obtained one more Pr—Al intermetallic compound (peak N') in the same melts than Tang [14]. This phenomenon might be due to the higher concentration of Pr(III) ions in ours, and there is enough Pr(III) ions to further generate Pr-rich intermetallic compound during the co-reduction process.

In general, comparing two curves with respect to molten LiCl—KCl eutectic containing PrCl<sub>3</sub>-AlCl<sub>3</sub> and PrCl<sub>3</sub>-AlCl<sub>3</sub>-ZnCl<sub>2</sub> salt systems, it is very likely that redox couple K/K' in Fig. 6b is formed by the reduction and depletion of Pr—Al intermetallic compound, and another pair of couple J/J' maybe be possibly caused by the under-potentially deposition of praseodymium on the aluminum and zinc alloy already coated onto the W electrode to form ternary Pr-Al-Zn intermetallic compound.

Interestingly, it is worth to mention that there is the only one redox signal for the Pr—Al intermetallic compound found between the redox couples B/B' and C/C' in the LiCl—KCl-PrCl<sub>3</sub>-AlCl<sub>3</sub>-ZnCl<sub>2</sub> system, while three signals corresponding to Er—Zn intermetallic compounds are observed. The electronegativity difference, adopted to predict the possibility of the formation of the intermetallic compound between two elements, could be the possible explanation for this phenomenon [54]. The greater the difference in electronegativity between two elements, the easier the formation for intermetallic compounds will be formed easily because the electronegativily difference between praseodymium and zinc is larger than that between praseodymium and aluminum, and the results that the introduction of AlCl<sub>3</sub> into LiCl—KCl-PrCl<sub>3</sub>-ZnCl<sub>2</sub> system has an insignificant influence on electrochemical properties of praseodymium are also obtained.

Fig. 7 displays the several OCP transient curves of LiCl–KCl-PrCl<sub>3</sub>-AlCl<sub>3</sub>-ZnCl<sub>2</sub> molten melts after the electrodepositing potential of  $-2.50\,\mathrm{V}$  or  $-2.60\,\mathrm{V}$  for  $10\,\mathrm{s}$  on the W electrodes at  $723\,\mathrm{K}$ . These curves feature a series of potential plateaux typical of the successive generation of different solid phases on the W electrode and all possess two large and stable potential plateaux at about  $-2.41\,\mathrm{V}$  and  $-1.98\,\mathrm{V}$  (plateaux A and B), which corresponds undoubtedly to the equilibrium potentials of Li(I)/Li and Pr(III)/Pr couples, respectively. Curve (II) reflects the OCP curve obtained in

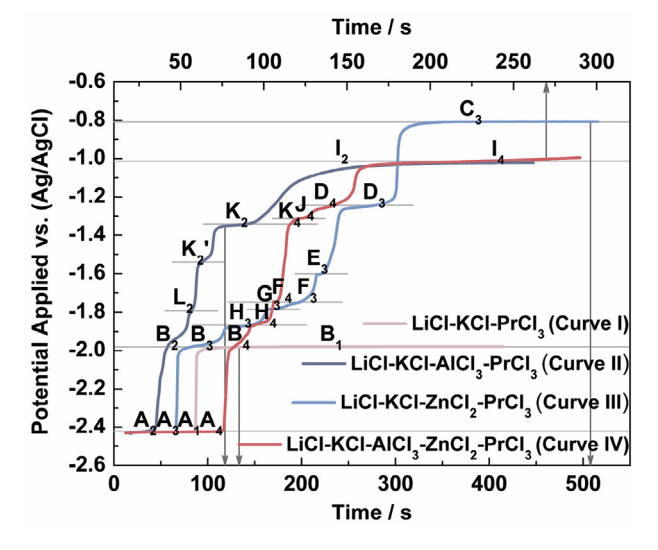


Fig. 7. OCP curves recorded on the W electrode in different molten salt systems under various deposition conditions: (I) PrCl<sub>3</sub> (1.1 wt%), (II) PrCl<sub>3</sub> (1.1 wt%)-AlCl<sub>3</sub> (0.2 wt%) and (III) PrCl<sub>3</sub> (1.1 wt%)-ZnCl<sub>2</sub> (0.2 wt%) after electrodepositing at -2.50 V for 10 s, and also (IV) PrCl<sub>3</sub> (1.1 wt%)-AlCl<sub>3</sub> (0.2 wt%)-ZnCl<sub>2</sub> (0.2 wt%) after electrodepositing at -2.60 V for 10 s in LiCl—KCl eutectic.

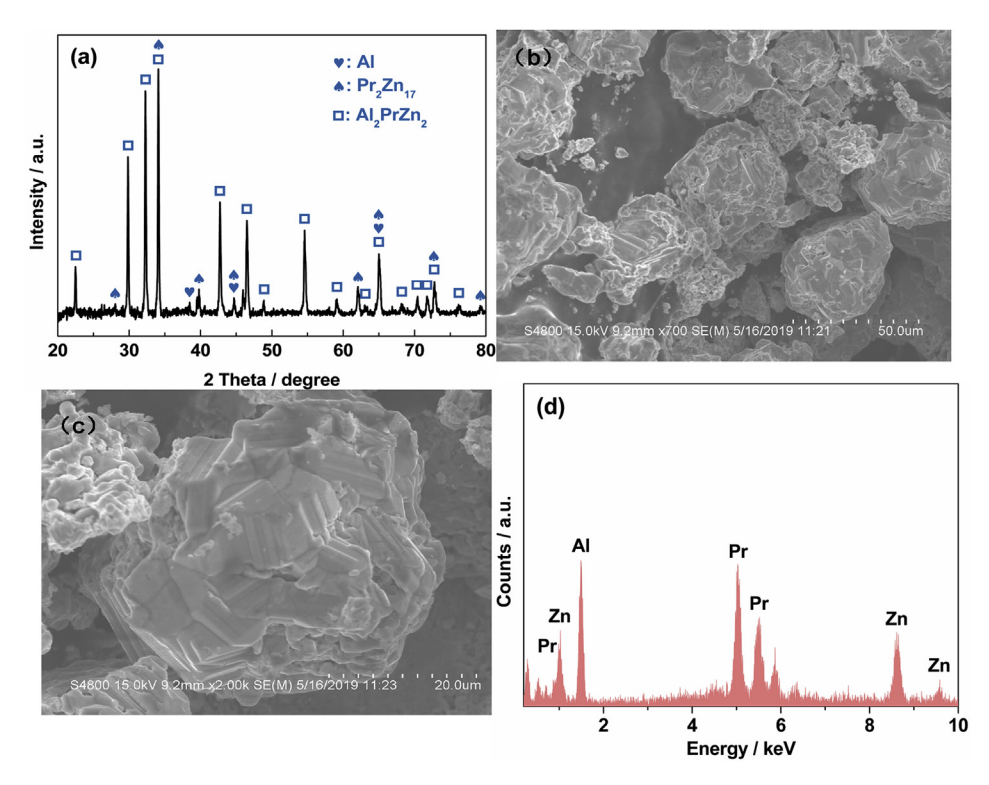


Fig. 8. XRD (a) and SEM-EDS (b, c, d) analyses of the cathodic deposits obtained in LiCl-KCl-PrCl<sub>3</sub>-AlCl<sub>3</sub>-ZnCl<sub>2</sub> melts on the molybdenum net electrode at 723 K.

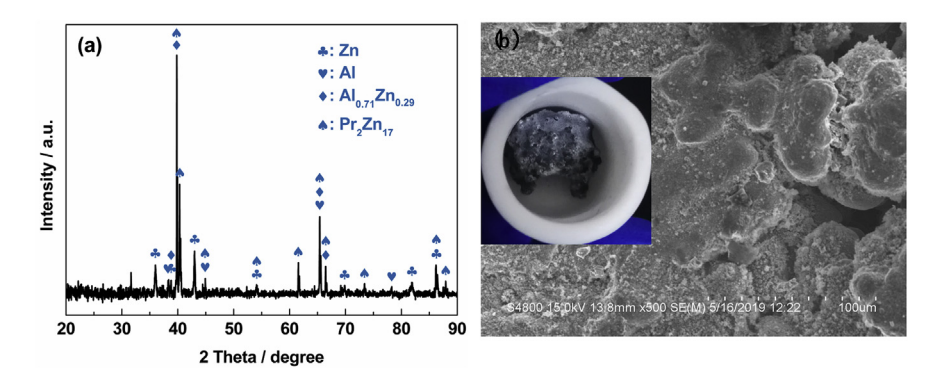


Fig. 9. XRD (a) and SEM (b) analyses of the galvanostatic (-6 mA) cathodic deposits collected in LiCl-KCl-PrCl<sub>3</sub> (2.02 wt%) melts at the liquid Al–Zn electrode at 783 K for 8 h.

molten LiCl-KCl-PrCl<sub>3</sub> (1.1 wt%) system with the solution of AlCl<sub>3</sub> (0.2 wt%) after affording a potential of -2.50 V for 10 s. Besides two confirmed potential plateaux A and B, however, three potential plateaux ( $K_2$ ,  $K_2$ ' and  $L_2$ ) are found at -1.34, -1.54 and -1.79 V ascribed to the successive dissolution of three Pr-Al intermetallic compounds, as also the plateau  $I_2$ , emerging at around  $-1.02 \, \text{V}$ , derives from the rest potential of the Al deposited on W electrode. As for the curve (III), the open circuit chronopotentiometry was carried out in LiCl-KCl eutectic by adding PrCl<sub>3</sub> (1.1 wt%)-ZnCl<sub>2</sub> (0.2 wt%) after electrodepositing at -2.50 V for 10 s, and reflected eight plateaux  $(A_3,\ C_3,\ D_3,\ E_3,\ F_3,\ G_3,\ H_3$  and  $B_3)$  at around -2.41, -0.81, -1.25, -1.60, -1.75, -1.79, -1.87 and -1.98 V, corresponding to the pure lithium metal striping, the pure zinc metal striping, the formation of Pr-Zn intermetallic compounds and pure Pr metal striping, respectively. Moreover, curve (IV) was recorded in the molten LiCl-KCl-PrCl<sub>3</sub> (1.1 wt%)-AlCl<sub>3</sub> (0.2 wt %)- $ZnCl_2$  (0.2 wt%) melts after electrodepositing at -2.60 V for 10 s. After comparing curves (II) and (III) with the one collected in LiCl-KCl-PrCl $_3$ -ZnCl $_2$ -AlCl $_3$  system (curve IV), apart from the seven confirmed potential plateaux (A $_4$ , I $_4$ , D $_4$ , K $_4$ , F $_4$ , H $_4$  and B $_4$ ) discovered above, one new potential plateau (J $_4$ ) are detected at nearly -1.32 V, which reasonably stems from the formation of ternary Pr-Al-Zn intermetallic compound. The comparison of reduction signal potentials collected from CV and OCP techniques is shown in Table 2, and the results obtained in OCPs are well reproduced with those attained from CVs in Fig. 6.

# 3.4. Preparation and characterization of the cathodic deposits

To confirm the cathodic products stemming from the coreduction process of Pr(III), Al(III) and Zn(III) ions on inert W electrode and the under potential deposition of Pr(III) ions at liquid Al—Zn electrode, potentiostatic and galvanostatic electrolyses were conducted to prepare alloy specimens with different electrode materials. After electrolysis process, the obtained specimens were washed using ethylene glycol and then stored inside the glove box

for further analyses.

Potentiostatic electrolysis experiment was implemented with the W electrode in the LiCl–KCl-PrCl<sub>3</sub>-AlCl<sub>3</sub>-ZnCl<sub>2</sub> molten melts at -1.5 V for 2 h at 723 K at first. There is only a small amount of Pr-Al-Zn alloys adhering on the W electrode although the experiment was repeated for several times. One reasonable explanation could be that all of intermetallic compounds deposited at this potential are based on W electrode coated with Zn metal, while at this temperature metal Zn was in the liquid state and might be easily drop from the W electrode during the electrolysis process.

Afterwards, the molybdenum net was adopted as the cathode, and the Pr-Al-Zn alloys were deposited by potentiostatic electrolysis at  $-1.5\,\text{V}$  for 2 h. Fig. 8a shows the XRD spectrum of the cathodic deposits collected in LiCl–KCl-PrCl<sub>3</sub>-AlCl<sub>3</sub>-ZnCl<sub>2</sub> system at 723 K, and also verifies that the components of the deposition product are Al metal as well as the intermetallic compounds Pr<sub>2</sub>Zn<sub>17</sub> and Al<sub>2</sub>PrZn<sub>2</sub> with tetragonal crystal system (I4/mmm). From Fig. 8b and c, it turns out that the morphology of Al<sub>2</sub>PrZn<sub>2</sub> intermetallic compound is lumpy shape. These lumps are formed by plenty of layers, and these layered structures are assembled tightly in a certain direction. The relative EDS analysis is shown in Fig. 8d, which confirms the existing of Pr. Al and Zn elements.

Moreover, galvanostatic ( $-6\,\text{mA}$ ) electrolysis experiment was carried out for 8 h at the liquid Al–Zn electrode in LiCl–KCl-PrCl<sub>3</sub> (2.02 wt%) melts at 783 K. Fig. 9 displays the XRD results of the surface of the cathodic product and SEM images. Besides the monophase of Al and Zn metals, the Al<sub>0.71</sub>Zn<sub>0.29</sub> and Pr<sub>2</sub>Zn<sub>17</sub> intermetallic compounds were identified as well.

### 4. Conclusions

The co-reduction behaviors of Pr(III) ions with both Al(III) and Zn(II) ions as well as the under potential deposition of Pr(III) ions at the liquid Al–Zn binary electrode were studied systematically in LiCl–KCl eutectic. In both cases, the reduction potential of Pr(III) ions occurs at more anodic potentials because of the decreasing of Pr activity in the metal phase. Meanwhile, the diffusion coefficients of Pr(III) ions in melt in the case of W electrode and liquid Al–Zn electrode were  $2.02 \times 10^{-5} \, \text{cm}^2/\text{s}$  and  $4.53 \times 10^{-5} \, \text{cm}^2/\text{s}$ , respectively, at  $100 \, \text{mV/s}$ . The results show that more Pr–Zn intermetallics could be formed than Pr–Al intermetallics. In addition, at the liquid Al–Zn electrode, Pr-Al-Zn alloys could be generated.

# **Declaration of competing interest**

The authors declared that they have no conflicts of interest to this work.

### Acknowledgements

This work was supported by the Major Program of National Natural Science Foundation of China (No. 21790373) and the general program of National Natural Science Foundation of China (No. 51604252).

### Appendix A. Supplementary data

Supplementary data to this article can be found online at https://doi.org/10.1016/j.electacta.2019.134971.

### References

 M. Gibilaro, L. Massot, R. Chamelot, P. Taxil, Co-reduction of aluminium and lanthanide ions in molten fluorides: application to cerium and samarium extraction from nuclear wastes, Electrochim. Acta 54 (2009) 5300-5306.

- [2] M. Kurata, N. Yahagi, S. Kitawaki, A. Nakayoshi, M. Fukushima, Sequential electrolysis of U-Pu alloy containing a small amount of am to recover U- and U-Pu-Am products, J. Nucl. Sci. Technol. 46 (2009) 175–183.
- [3] K. Kinoshita, K. Tadafumi, I. Tadashi, M. Ougier, J.P. Glatz, Separation of actinides from rare earth elements by means of molten salt electrorefining with anodic dissolution of U-Pu-Zr alloy fuel, J. Phys. Chem. Solids 66 (2005) 619–624.
- [4] O. Shirai, T. Iwai, K. Shiozawa, Y. Suzuki, Y. Sakamura, T. Inoue, Electrolysis of plutonium nitride in LiCl-KCl eutectic melts, J. Nucl. Mater. 277 (2000) 226–230.
- [5] P. Soucek, L. Cassayre, R. Malmbeck, E. Mendes, R. Jardin, J.P. Glatz, Electrorefining of U-Pu-Zr-alloy fuel onto solid aluminium cathodes in molten LiCl-KCl. Radiochim. Acta 96 (2008) 315–322.
- [6] T. Koyama, M. Iizuka, Y. Shoji, R. Fujita, H. Tanaka, T. Kobayashi, M. Tokiwai, An experimental study of molten salt electrorefining of uranium using solid iron cathode and liquid cadmium cathode for development of pyrometallurgical reprocessing, J. Nucl. Sci. Technol. 34 (1997) 384–393.
- [7] M. Iizuka, K. Uozumi, T. Inoue, T. Iwai, O. Shirai, Y. Arai, Behavior of plutonium and americium at liquid cadmium cathode in molten LiCl-KCl electrolyte, J. Nucl. Mater. 299 (2001) 32–42.
- [8] D. Hudry, I. Bardez, A. Rakhmatullin, C. Bessada, F. Bart, S. Jobic, P. Deniard, Synthesis of rare earth phosphates in molten LiCl-KCl eutectic: application to preliminary treatment of chlorinated waste streams containing fission products, J. Nucl. Mater. 381 (2008) 284–289.
- [9] Y. Castrillejo, M.R. Bermejo, P.D. Arocas, A.M. Martinez, E. Barrado, Electrochemical behaviour of praseodymium (III) in molten chlorides, J. Electroanal. Chem. 575 (2005) 61–74.
- [10] T. Nohira, H. Kambara, K. Amezawa, Y. Ito, Electrochemical formation and phase control of Pr-Ni alloys in a molten LiCl-KCl-PrCl<sub>3</sub> system, J. Electrochem. Soc. 152 (2005) C183—C189.
- [11] Z.Y. Qiao, S. Duan, D. Inman, Electrochemical reduction of praseodymium chloride in LiCl-KCl melt, J. Appl. Electrochem. 19 (1989) 937–939.
- [12] H. Tang, H. Deng, Q. Ren, D. Cai, Y. Ren, L. Shao, Y. Yan, M. Zhang, Electro-chemical behavior of praseodymium and Pr-Al intermetallics in LiCl-KCl-AlCl<sub>3</sub>-PrCl<sub>3</sub> melts, J. Rare Earths 34 (2016) 428–434.
- [13] Y. Castrillejo, R. Bermejo, A.M. Martinez, E. Barrado, P. Diaz Arocas, Application of electrochemical techniques in pyrochemical processes - electrochemical behaviour of rare earths at W, Cd, Bi and Al electrodes, J. Nucl. Mater. 360 (2007) 32—42.
- [14] H. Tang, Y.D. Yan, M.L. Zhang, X. Li, Y. Huang, Y.L. Xu, Y. Xue, W. Han, Z.J. Zhang, AlCl<sub>3</sub>-aided extraction of praseodymium from Pr<sub>6</sub>O<sub>11</sub> in LiCl-KCl eutectic melts, Electrochim. Acta 88 (2013) 457–462.
- [15] Y. Xue, D.B. Ji, Y.D. Yan, M.L. Zhang, Y.H. Liu, P. Wang, T.Q. Yin, P. Li, Y. Zhao, J. Wang, Electrochemical extraction of praseodymium by formation of Zn-Pr alloy in LiCl-KCl melts with the assistance of ZnCl<sub>2</sub> and liquid Zn, J. Electrochem. Soc. 164 (2017) D253—D262.
- [16] M. Li, J. Wang, W. Han, X.G. Yang, M. Zhang, Y. Sun, M.L. Zhang, Y.D. Yan, Electrochemical formation and thermodynamic evaluation of Pr-Zn intermetallic compounds in LiCl-KCl eutectic melts, Electrochim. Acta 228 (2017) 299–307
- [17] Y. Castrillejo, M.R. Bermejo, P.D. Arocas, A.M. Martinez, E. Barrado, The electrochemical behaviour of the Pr(III)/Pr redox system at Bi and Cd liquid electrodes in molten eutectic LiCl-KCl, J. Electroanal. Chem. 579 (2005) 343–358.
- [18] T. Jiang, S.M. Peng, M. Li, T.T. Pei, W. Han, Y. Sun, M.L. Zhang, Electrochemical behavior of Pr(III) ions on a Bi-coated W electrode in LiCl-KCl melts, Acta Physico-Chim. Sin. 32 (2016) 1708–1714.
- [19] T.Q. Yin, K. Liu, Y.L. Liu, Y.D. Yan, G.L. Wang, Z.F. Chai, W.Q. Shi, Electrochemical and thermodynamic properties of Pr on the liquid Bi electrode in LiCl-KCl eutectic melt, J. Electrochem. Soc. 165 (2018) D452—D460.
- [20] T.Q. Yin, Y.L. Liu, L. Wang, Y.D. Yan, G.L. Wang, Z.F. Chai, W.Q. Shi, Thermodynamic properties of praseodymium on the liquid cadmium electrode and evaluation of anodic dissolution behavior in LiCl-KCl eutectic, J. Nucl. Mater. 523 (2019) 16–25.
- [21] H. Tang, Y.D. Yan, M.L. Zhang, X. Li, W. Han, Y. Xue, Z.J. Zhang, H. He, Fabrication of Mg-Pr and Mg-Li-Pr alloys by electrochemical co-reduction from their molten chlorides, Electrochim. Acta 107 (2013) 209–215.
- [22] T.Q. Yin, Y. Liang, J.M. Qu, P. Li, R.F. An, Y. Xue, M.L. Zhang, W. Han, G.L. Wang, Y.D. Yan, Thermodynamic and electrochemical properties of praseodymium and the formation of Ni-Pr intermetallics in LiCl-KCl melts, J. Electrochem. Soc. 164 (2017) D835—D842.
- [23] T.Q. Yin, Y. Xue, Y.D. Yan, Y.H. Zheng, Y.L. Song, G.L. Wang, M.L. Zhang, M. Qiu, D.H. Hu, Electrochemical synthesis and thermodynamic properties of Pr-Ni intermetallic compounds in a LiCl-KCl-NiCl<sub>2</sub>-PrCl<sub>3</sub> melt, ChemElectroChem 6 (2019) 876–884.
- [24] O. Conocar, N. Douyere, J. Lacquement, Distribution of actinides and lanthanides in a molten fluoride/liquid aluminum alloy system, J. Alloy. Comp. 389 (2005) 29–33.
- [25] L. Rault, M. Heusch, M. Allibert, F. Lemort, X. Deschanel, R. Boen, Test of actinide-lanthanide separation in an aluminum-based pyrochemical system, Nucl. Technol. 139 (2002) 167–174.
- [26] O. Conocar, N. Douyere, J.P. Glatz, J. Lacquement, R. Malmbeck, J. Serp, Promising pyrockemical actinide/lanthanide separation processes using aluminum, Nucl. Sci. Eng. 153 (2006) 253–261.
- [27] K. Liu, Y.L. Liu, L.Y. Yuan, H. He, Z.Y. Yang, X.L. Zhao, Z.F. Chai, W.Q. Shi,

- Electroextraction of samarium from  $\mbox{Sm}_2\mbox{O}_3$  in chloride melts, Electrochim. Acta 129 (2014) 401–409.
- [28] K. Liu, Y.L. Liu, L.Y. Yuan, L. Wang, L. Wang, Z.J. Li, Z.F. Chai, W.Q. Shi, Thermodynamic and electrochemical properties of holmium and Ho<sub>x</sub>Al<sub>y</sub> intermetallic compounds in the LiCl-KCl eutectic, Electrochim. Acta 174 (2015) 15–25
- [29] K. Liu, Y.L. Liu, L.Y. Yuan, X.L. Zhao, Z.F. Chai, W.Q. Shi, Electroextraction of gadolinium from Gd<sub>2</sub>O<sub>3</sub> in LiCl-KCl-AlCl<sub>3</sub> molten salts, Electrochim. Acta 109 (2013) 732–740.
- [30] K. Liu, Y.L. Liu, L.Y. Yuan, X.L. Zhao, H. He, G.A. Ye, Z.F. Chai, W.Q. Shi, Electrochemical formation of erbium-aluminum alloys from erbia in the chloride melts, Electrochim, Acta 116 (2014) 434—441.
- [31] Y.L. Liu, L.Y. Yuan, G.A. Ye, K. Liu, L. Zhu, M.L. Zhang, Z.F. Chai, W.Q. Shi, Coreduction behaviors of lanthanum and aluminium ions in LiCl-KCl eutectic, Electrochim. Acta 147 (2014) 104–113.
- [32] Y.L. Liu, K. Liu, L.X. Luo, L.Y. Yuan, Z.F. Chai, W.Q. Shi, Direct separation of uranium from lanthanides (La, Nd, Ce, Sm) in oxide mixture in LiCl-KCl eutectic melt, Electrochim. Acta 275 (2018) 100—109.
- [33] Y.L. Liu, L.X. Luo, N. Liu, B.L. Yao, K. Liu, L.Y. Yuan, Z.F. Chai, W.Q. Shi, A particularly simple NH<sub>4</sub>Cl-based method for the dissolution of UO<sub>2</sub> and rare earth oxides in LiCl-KCl melt under air atmosphere, J. Nucl. Mater. 508 (2018) 63–73
- [34] Y.L. Liu, G.A. Ye, K. Liu, L.Y. Yuan, Z.F. Chai, W.Q. Shi, Electrochemical behavior of La(III) on the zinc-coated W electrode in LiCl-KCl eutectic, Electrochim. Acta 168 (2015) 206–215.
- [35] Y.L. Liu, L.Y. Yuan, L. Kui, G.A. Ye, M.L. Zhang, H. He, H.B. Tang, R.S. Lin, Z.F. Chai, W.Q. Shi, Electrochemical extraction of samarium from LiCl-KCl melt by forming Sm-Zn alloys, Electrochim. Acta 120 (2014) 369–378.
- [36] L.X. Luo, Y.L. Liu, N. Liu, K. Liu, J.W. Pang, L.Y. Yuan, Z.F. Chai, W.Q. Shi, Kinetics process of Tb(III)/Tb couple at liquid Zn electrode and thermodynamic properties of Tb-Zn alloys formation, Sci. China Chem. 60 (2017) 813–821.
- [37] L.X. Luo, Y.L. Liu, N. Liu, L. Wang, L.Y. Yuan, Z.F. Chai, W.Q. Shi, Electrochemical and thermodynamic properties of Nd(III)/Nd(0) couple at liquid Zn electrode in LiCl-KCl melt, Electrochim. Acta 191 (2016) 1026–1036.
- [38] H. Tang, B. Pesic, Electrochemistry of ErCl<sub>3</sub> and morphology of erbium electrodeposits produced on Mo substrate in early stages of electrocrystallization from LiCl-KCl molten salts, Electrochim. Acta 133 (2014) 224–232.
- [39] Z. Chen, M.L. Zhang, W. Han, Z.Y. Hou, Y.D. Yan, Electrodeposition of Li and electrochemical formation of Mg—Li alloys from the eutectic LiCl—KCl, J. Alloy. Comp. 464 (2008) 174–178.
- [40] D. Pletcher, R. Greff, R. Peat, L.M. Peter, J. Robinson, Instrumental Methods in

- Electrochemistry, Southampton Electrochemistry Group, University of Southampton, Horwood, London, 2001.
- [41] T. Støre, G. Haarberg, R. Tunold, Determination of diffusion coefficients of depositing ions in molten chlorides by transient electrochemical techniques, J. Appl. Electrochem. 30 (2000) 1351–1360.
- [42] G.Y. Kim, D. Yoon, S. Paek, S.H. Kim, T.J. Kim, D.H. Ahn, A study on the electrochemical deposition behavior of uranium ion in a LiCl-KCl molten salt on solid and liquid electrode, J. Electroanal. Chem. 682 (2012) 128–135.
- [43] S.L. Jiang, K. Liu, Y.L. Liu, T.Q. Yin, Z.F. Chai, W.Q. Shi, Electrochemical behavior of Th(IV) on the bismuth electrode in LiCl–KCl eutectic, J. Nucl. Mater. 523 (2019) 268–275.
- [44] G.M. Haarberg, T. Støre, R. Tunold, Metal deposition from chloride melts: I. Rates of diffusion in solvent melt, Electrochim. Acta 76 (2012) 256–261.
- [45] Y. Castrillejo, A. Martínez, M. Vega, E. Barrado, G. Picard, Electrochemical study of the properties of iron ions in ZnCl<sub>2</sub>+2NaCl melt at 450°C, I. Electroanal. Chem. 397 (1995) 139–147.
- [46] J. Imbeaux, J. Saveant, Convolutive potential sweep voltammetry: I. Introduction, J. Electroanal. Chem. Interfacial Electrochem. 44 (1973) 169–187.
- [47] J. Saveant, D. Tessier, Convolution potential sweep voltammetry V. Determination of charge transfer kinetics deviating from the Butler-Volmer behaviour, J. Electroanal. Chem. Interfacial Electrochem. 65 (1975) 57–66.
- [48] M. Mohamedi, N. Kawaguchi, Y. Sato, T. Yamamura, Electrochemical study of the mechanism of formation of the surface alloy of aluminum-niobium in LiCl-KCl eutectic melt, J. Alloy. Comp. 287 (1999) 91–97.
- [49] M. Goto, K.B. Oldham, Semiintegral electroanalysis. Shapes of neopolarograms, Anal. Chem. 45 (1973) 2043–2050.
- [50] P. Wang, D.B. Ji, D.Q. Ji, J.N. Zheng, Y.D. Yan, M.L. Zhang, W. Han, H.J. Wu, Electrochemical and thermodynamic properties of ytterbium and formation of Zn-Yb alloy on liquid Zn electrode, J. Nucl. Mater. 517 (2019) 157–164.
- [51] H. Ren, Y.L. Liu, T.Q. Yin, Z.X. Deng, D.W. Yang, Z.F. Chai, K.K. Chang, W.Q. Shi, Electrochemical deposition of erbium on a binary Al-Zn cathode, J. Electrochem. Soc. 166 (2019) D569–D576.
- [52] H. Tang, B. Pesic, Electrochemical behavior of LaCl<sub>3</sub> and morphology of La deposit on molybdenum substrate in molten LiCl–KCl eutectic salt, Electrochim. Acta 119 (2014) 120–130.
- [53] A.J. Bard, L.R. Faulkner, Electrochemical Methods: Fundamentals and Applications, Wiley, New York, 2001.
- [54] V. Smolenski, A. Novoselova, Electrochemistry of redox potential of the couple Tm<sup>3+</sup>/Tm<sup>2+</sup> and the formation of a Tm-Al alloy in fused NaCl-2CsCl eutectic, Electrochim. Acta 63 (2012) 179–184.